

# A Hybrid Approach to Spectral Reconstruction of Piecewise Smooth Functions

Anne Gelb<sup>1</sup>

*Received October 26, 2000; final December 7, 2000*

---

Consider a piecewise smooth function for which the (pseudo-)spectral coefficients are given. It is well known that while spectral partial sums yield exponentially convergent approximations for smooth functions, the results for piecewise smooth functions are poor, with spurious oscillations developing near the discontinuities and a much reduced overall convergence rate. This behavior, known as the Gibbs phenomenon, is considered as one of the major drawbacks in the application of spectral methods. Various types of reconstruction methods developed for the recovery of piecewise smooth functions have met with varying degrees of success. The Gegenbauer reconstruction method, originally proposed by Gottlieb *et al.* has the particularly impressive ability to reconstruct piecewise analytic functions with exponential convergence up to the points of discontinuity. However, it has been sharply criticized for its high cost and susceptibility to round-off error. In this paper, a new approach to Gegenbauer reconstruction is considered, resulting in a reconstruction method that is less computationally intensive and costly, yet still enjoys superior convergence. The idea is to create a procedure that combines the well known exponential filtering method in smooth regions away from the discontinuities with the Gegenbauer reconstruction method in regions close to the discontinuities. This hybrid approach benefits from both the simplicity of exponential filtering and the high resolution properties of the Gegenbauer reconstruction method. Additionally, a new way of computing the Gegenbauer coefficients from Jacobian polynomial expansions is introduced that is both more cost effective and less prone to round-off errors.

---

**KEY WORDS:** Fourier expansion; Gibbs phenomenon; piecewise smoothness; reconstruction.

---

<sup>1</sup> Department of Mathematics, P.O. Box 871804, Arizona State University, Tempe, Arizona 85287-1804. E-mail: ag@math.la.asu.edu

## 1. INTRODUCTION

Consider a periodic piecewise smooth function  $f(x)$  defined in  $[-1, 1]$  for which the (pseudo-)spectral coefficients are given. It is well known that while spectral partial sums yield exponentially convergent approximations for smooth functions, the results for piecewise smooth functions are poor, with spurious oscillations developing near the discontinuities and a much reduced overall convergence rate of  $\mathcal{O}(1/N)$ . This behavior, known as the Gibbs phenomenon, is considered as one of the major drawbacks in the application of spectral methods. There is ample literature devoted to this problem, for example, consult [1, 4, 6, 7, 13, 15, 16, 22], and references therein. While a number of methods have shown moderate success, the Gegenbauer reconstruction method, originally proposed by Gottlieb *et al.* in [15], has the particularly impressive ability to reconstruct piecewise analytic functions with exponential convergence *up to* the points of discontinuity. Furthermore, the Gegenbauer reconstruction method has been developed not only for recovering functions when the given information comes from the Fourier (pseudo-)spectral coefficients, but is also applicable when the general Jacobi polynomial expansion for the function in each smooth sub-interval is known [14]. This makes the Gegenbauer reconstruction method amenable for a large class of physical applications.

Like all other high order reconstruction methods, the Gegenbauer reconstruction method requires an a priori knowledge of the locations of the jump discontinuities. Much attention has been devoted to the topic of edge detection, for instance consult [3, 8, 9, 17, and 19] for spectral data edge detection techniques. In [8] and [9] an edge detection technique was developed that successfully identifies the jump locations from either the Fourier or the general Jacobi polynomial partial sum expansions. After successfully locating all of the jump discontinuities, application of the Gegenbauer reconstruction method ensures both the complete removal of the Gibbs phenomenon and restoration of spectral accuracy in the maximum norm for piecewise analytic functions.

One of the criticisms of the Gegenbauer reconstruction method is its susceptibility to round-off error due to the rapid growth of the Gegenbauer polynomials. Not only is the theoretical exponential convergence unrealizable, but the round-off error may completely ruin the approximation. The other main criticism involves the high cost of computing the Gegenbauer coefficients. This is particularly problematic in the Jacobi polynomial expansion case, and also becomes an issue for all higher dimension approximations. In this paper, a new approach to Gegenbauer reconstruction is considered, resulting in a reconstruction method that is less computationally intensive and costly, yet still enjoys superior convergence. The idea is to create a

procedure that combines the well known exponential filtering method in smooth regions away from the discontinuities with the Gegenbauer reconstruction method in regions close to the discontinuities. This hybrid approach benefits from both the simplicity of exponential filtering and the high resolution properties of the Gegenbauer reconstruction method. Additionally, a new way of computing the Gegenbauer coefficients from Jacobian polynomial expansions is introduced that is both more cost effective and less prone to round-off errors.

This paper is organized as follows: In Section 2 the edge detection techniques from [8] and [9] are reviewed for both the Fourier and Legendre expansion cases, as well as for the extension to two dimensions. In Section 3, we discuss the recovery of piecewise smooth functions using both exponential filtering and the Gegenbauer reconstruction method. The hybrid Gegenbauer reconstruction method is then introduced. Numerical applications are presented in Section 4.

## 2. EDGE DETECTION OF PIECEWISE SMOOTH FUNCTIONS FROM SPECTRAL DATA

As mentioned above, critical to all high resolution reconstruction methods is the a priori knowledge of the locations of the jump discontinuities. Much research has been devoted to the topic of edge detection. Here we utilize the method developed in [8] and [9] for Fourier and Legendre spectral data. This two step method first detects the neighborhoods of the jump discontinuities and then “pinpoints” the exact locations by a nonlinear enhancement procedure. Details can be found in [8] and [9].

### 2.1. The Fourier Expansion Case

Consider a piecewise smooth function  $f(x)$  defined in  $[-1, 1]$ , that has a finite number of jump discontinuities of the first kind with well defined one-sided limits,  $f(x \pm) = \lim_{x \rightarrow x \pm} f(x)$ . Let  $[f](x) := f(x+) - f(x-)$  denote the local jump function. Recall the Fourier partial sum expansion

$$S_N[f](x) = \sum_{k=-N}^N \hat{f}_k e^{ik\pi x} \quad (2.1)$$

based on the continuous Fourier coefficients,

$$\hat{f}_k = \frac{1}{2} \int_{-1}^1 f(x) e^{-ik\pi x} dx$$

We wish to detect the jump discontinuities of  $f(x)$  from its Fourier partial sum expansion (2.1). To this end, we refer to the concentration method derived in [8] based on the odd kernel  $K_N^\sigma(t)$ . The kernel is designed so that the support of  $K_N^\sigma * f$  tends to the singular support of  $f$ , specifically yielding the concentration property

$$K_N^\sigma * f(x) \rightarrow [f](x), \quad \text{as } N \rightarrow \infty \quad (2.2)$$

This “concentration” kernel is written as

$$K_N^\sigma(t) = - \sum_{k=1}^N \sigma\left(\frac{k}{N}\right) \sin kt$$

where  $\sigma(k/N)$  are the concentration factors satisfying

$$\frac{\sigma(\xi)}{\xi} \in C^2[0, 1]$$

It was shown that if the concentration factors  $\sigma(\xi)$  are normalized so that

$$\int_0^1 \frac{\sigma(\xi)}{\xi} d\xi = 1$$

then the concentration property (2.2) holds with the estimate

$$|K_N^\sigma * S_N(f) - [f](x)| \leq \text{Const} \cdot \frac{\log N}{N}$$

The concentration method for detecting edges is implemented as

$$S_N^\sigma[f](x) := i\pi \sum_{k=-N}^N \text{sgn}(k) \sigma\left(\frac{|k|}{N}\right) \hat{f}_k e^{ik\pi x} \quad (2.3)$$

Several examples of admissible concentration factors can be found in [9]. Due to its rapid convergence away from the discontinuities, the exponential concentration factor,

$$\sigma^{\text{exp}} = \sigma(\xi) = \text{Const} \cdot \xi e^{1/(\alpha\xi(\xi-1))}, \quad \text{Const} = \int \exp\left(\frac{-1}{\alpha\eta(\eta-1)}\right) d\eta \quad (2.4a)$$

with  $\sigma(0) = \sigma(1) = 0$ , is particularly effective.

As an example, consider the function

**Example 2.1.**

$$f(x) = \begin{cases} \cos \frac{\pi}{2} x, & -1 \leq x < -\frac{1}{2} \\ x^3 - \sin \frac{3\pi}{2} x + 1, & -\frac{1}{2} \\ x^2 + 4x^3 - 5x, & \frac{1}{2} \leq x \leq 1 \end{cases} \quad (2.4b)$$

As seen in Fig. 2.1, Example 2.1 has two jump discontinuities and

$$[f](x) = \begin{cases} 0.875, & \text{if } x = -\frac{1}{2} \\ -2.17, & \text{if } x = \frac{1}{2} \\ 0, & \text{otherwise} \end{cases} \quad (2.5)$$

Application of the concentration method (2.3) is seen in Fig. 2.2. While it is clear that the neighborhoods of the discontinuities are located around

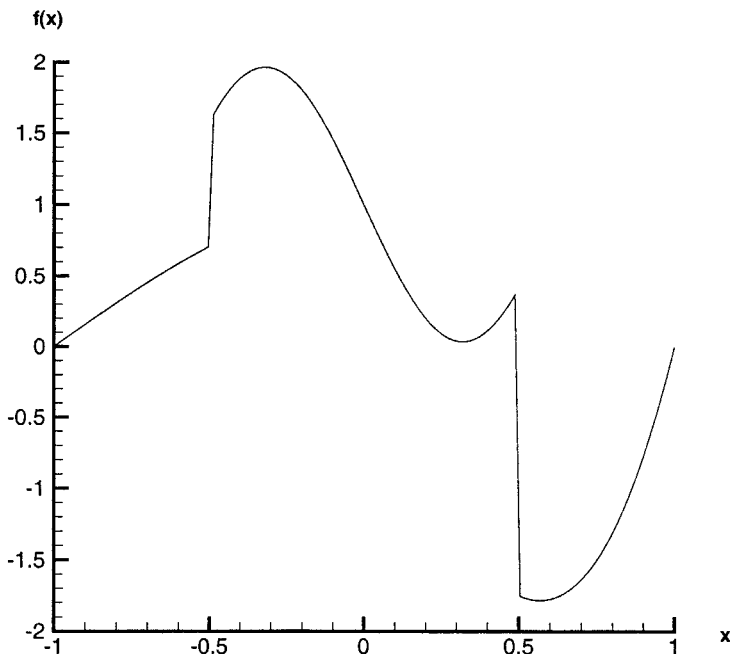


Fig. 2.1. Plot of Example 2.1.

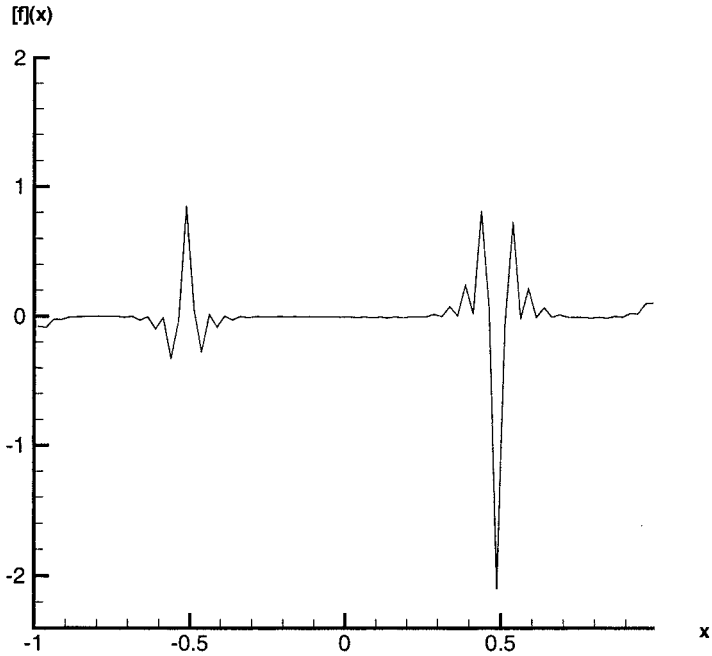


Fig. 2.2. Application of the concentration method (2.3) for Example 2.1 using 80 collocated Fourier coefficients.

$x = -\frac{1}{2}$  and  $x = \frac{1}{2}$ , a follow up step is necessary to “pinpoint” the exact jump locations. This is accomplished by applying the nonlinear enhancement procedure [9], which amplifies the separation of scales resulting from (2.3). More specifically, let  $\{x_j^*\}_{j=1}^M$  denote the locations of the jump discontinuities of  $f(x)$ . Then (2.3) is amplified by

$$(S_N^\sigma[f](x))^q = \begin{cases} ([f](x_j^*))^q, & \text{if } x = x_j^* \\ \mathcal{O}\left(\frac{1}{N}\right)^q, & \text{if } x \neq x_j^* \end{cases}$$

A more pronounced separation of scales is easily accomplished by defining

$$T := N^{q/2}(S_N^\sigma[f](x))^q \rightarrow \begin{cases} N^{q/2}([f](x_j^*))^q, & \text{if } x = x_j^* \\ \mathcal{O}(N^{-q/2}), & \text{if } x \neq x_j^* \end{cases}$$

The enhanced edge detection method is then

$$T_N(S_N^\sigma[f](x)) = \begin{cases} S_N^\sigma[f](x), & \text{if } |T| > J_{\text{crit}} \\ 0, & \text{if } |T| < J_{\text{crit}} \end{cases} \tag{2.6}$$

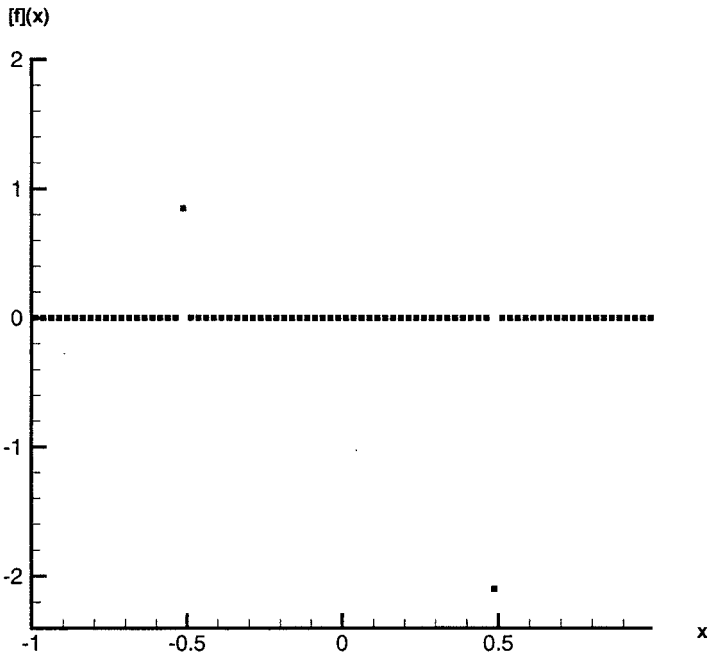


Fig. 2.3. Application of the enhanced edge detection method for Example 2.1 using 80 collocated Fourier coefficients.

where  $J_{\text{crit}}$  is an  $\mathcal{O}(1)$  global threshold parameter signifying the minimal amplitude for the jump discontinuity not to be negligible. Since (2.3) actually locates the neighborhoods of the discontinuities, the exact jump locations are determined as the corresponding locations to the largest amplitudes  $|T| > J_{\text{crit}}$  in each neighborhood of admissible jumps (i.e., where  $|T| > J_{\text{crit}}$ ). Note that  $J_{\text{crit}}$  should be chosen to be consistent with the variation and scaling of the function, and experiments show that  $q=2$  is adequate for enhancement. The results of the enhancement procedure (2.6) are shown in Fig. 2.3, where it is clear that the jump locations have been correctly identified.

## 2.2. The Legendre Expansion Case

Now suppose the Legendre expansion coefficients of a piecewise smooth function  $f(x)$  are known. The continuous Legendre polynomial partial sum expansion is given by

$$S_N(f)(x) = \sum_{k=0}^N \hat{f}_k P_k(x)$$

where

$$\hat{f}_k = \frac{2k+1}{2} \int_{-1}^1 f(x) P_k(x) dx$$

To derive the concentration property for the Legendre case, we first recall an example of an admissible concentration factor given for the Fourier case,  $\sigma(\xi) = \xi$  [8]. The resulting concentration sum (2.3) is then

$$\begin{aligned} S_N^\sigma[f](x) &= i\pi \sum_{k=-N}^N \operatorname{sgn}(k) \frac{|k|}{N} \hat{f}_k e^{ik\pi x} \\ &= \frac{1}{N} \sum_{k=-N}^N ik\pi \hat{f}_k e^{ik\pi x} \\ &= \frac{1}{N} \frac{d}{dx} S_N(f)(x) \end{aligned}$$

Thus essentially we are looking at the derivative of the spectral projection of  $f(x)$  to determine the locations of the jump discontinuities. In [9] this idea instigated the development of an edge detection method for general Jacobi expansions, which amounts to computing

$$\frac{\pi \sqrt{1-x^2}}{N} \frac{d}{dx} S_N(f)(x) = \frac{\pi \sqrt{1-x^2}}{N} \sum_{k=0}^N \hat{f}_k \frac{d}{dx} P_k(x) \rightarrow [f](x) \quad (2.7)$$

for which the estimate holds:

$$\begin{aligned} &\left| \frac{\pi \sqrt{1-x^2}}{N} \frac{d}{dx} S_N(f)(x) - [f](x) \right| \\ &\leq K \cdot \frac{\log N}{N(1-x^2)^{1/4}}, \quad -1 + K \cdot \frac{1}{N^2} < x < 1 - K \cdot \frac{1}{N^2} \end{aligned}$$

Examples for the Chebyshev and Legendre cases can be found in [9]. The nonlinear enhancement (2.6) is performed as in the Fourier case.

### 2.3. Edge Detection in Two Dimensions

It is possible to employ the edge detection and enhancement procedures in two dimensions by fixing the variable in one direction and determining the edges in the other direction as a function of the fixed variable.

In the Fourier case, the jump discontinuities of  $f(x, y)$  for each fixed  $\bar{x}$  and  $\bar{y}$  are determined by utilizing (2.3) as

$$\begin{aligned}
 S_N^\sigma[f](x(\bar{y})) &= \pi i \sum_{l=-N}^N \sum_{k=-N}^N \operatorname{sgn}(k) \sigma\left(\frac{|k|}{N}\right) \hat{f}_{k,l} e^{ik\pi x(\bar{y}) + il\pi \bar{y}} \\
 &\rightarrow [f](x_i^*(\bar{y})), \quad i = 1, \dots, M_x(\bar{y}) \\
 S_N^\sigma[f](y(\bar{x})) &= \pi i \sum_{l=-N}^N \sum_{k=-N}^N \operatorname{sgn}(l) \sigma\left(\frac{|l|}{N}\right) \hat{f}_{k,l} e^{ik\pi \bar{x} + il\pi y(\bar{x})} \\
 &\rightarrow [f](y_j^*(\bar{x})), \quad j = 1, \dots, M_y(\bar{x})
 \end{aligned} \tag{2.8}$$

where  $\hat{f}_{k,l}$  are the Fourier coefficients

$$\hat{f}_{k,l} := \frac{1}{4} \int_{-1}^1 \int_{-1}^1 f(x, y) e^{-in(kx + ly)} dy dx$$

and

$$x_i^*(\bar{y}), \quad i = 1, \dots, M_x(\bar{y}), \quad y_j^*(\bar{x}), \quad j = 1, \dots, M_y(\bar{x})$$

represent the finite jump discontinuities in each fixed direction. As an example, consider the function

**Example 2.2.**

$$f(x, y) = \begin{cases} 3x + 2y^2 + 3, & \text{if } x^2 + y^2 < (0.5)^2 \\ 0, & \text{otherwise} \end{cases} \tag{2.9}$$

shown in Fig. 2.4. The concentration method (2.8) is applied with  $\sigma = \sigma^{\text{exp}}$  (2.4a) in each direction on the fixed values  $\bar{x}_j = -1 + 2(j/N)$ ,  $\bar{y}_k = -1 + 2(k/N)$ ,  $j, k = 1, \dots, N$ . Figure 2.5 shows the convergence to the jump discontinuities of  $[f](x, y)$  occurring at  $x^2 + y^2 = (0.5)^2$  for Example 2.2. While the neighborhoods of the discontinuities are indeed detected, the process must be further enhanced by performing (2.6) in each direction, and hence one computes

$$\begin{aligned}
 T_x &:= N^{q/2} (S_N^\sigma[f](x(\bar{y})))^q \\
 &\rightarrow \begin{cases} N^{q/2} ([f](x_i^*(\bar{y})))^q, & \text{if } x = x_i^*(\bar{y}), \quad i = 1, \dots, M_x(\bar{y}) \\ \mathcal{O}(N^{-q/2}), & \text{if } x \neq x_i^*(\bar{y}), \quad i = 1, \dots, M_x(\bar{y}) \end{cases} \\
 T_y &:= N^{q/2} (S_N^\sigma[f](y(\bar{x})))^q \\
 &\rightarrow \begin{cases} N^{q/2} ([f](y_j^*(\bar{x})))^q, & \text{if } y = y_j^*(\bar{x}), \quad j = 1, \dots, M_y(\bar{x}) \\ \mathcal{O}(N^{-q/2}), & \text{if } y \neq y_j^*(\bar{x}), \quad j = 1, \dots, M_y(\bar{x}) \end{cases}
 \end{aligned} \tag{2.10}$$

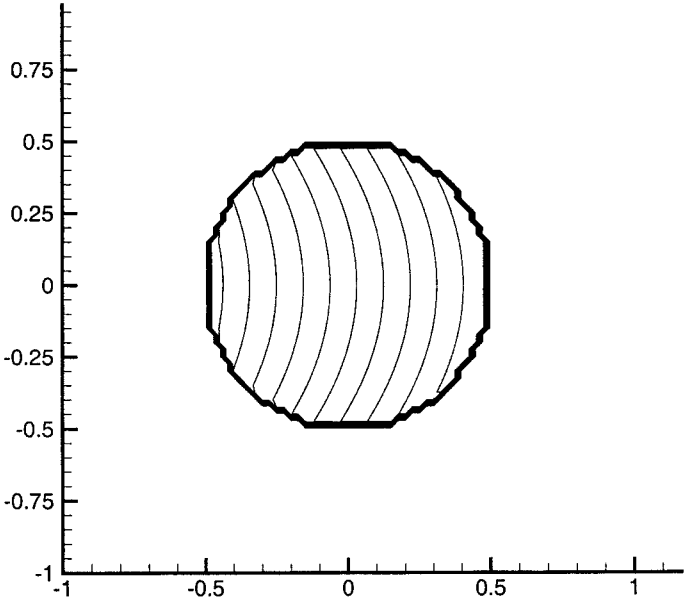


Fig. 2.4. Plot of Example 2.2.

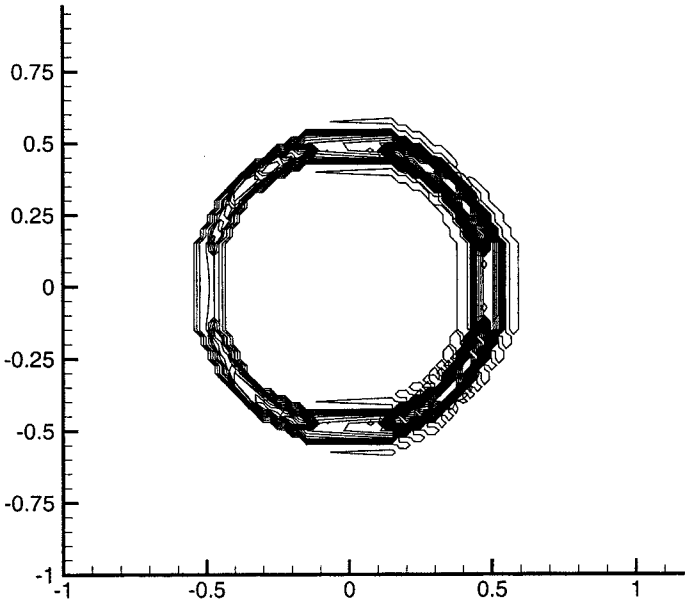


Fig. 2.5. Application of the concentration method (2.3) for Example 2.2 using  $N=80$  collocated Fourier coefficients in each fixed direction.

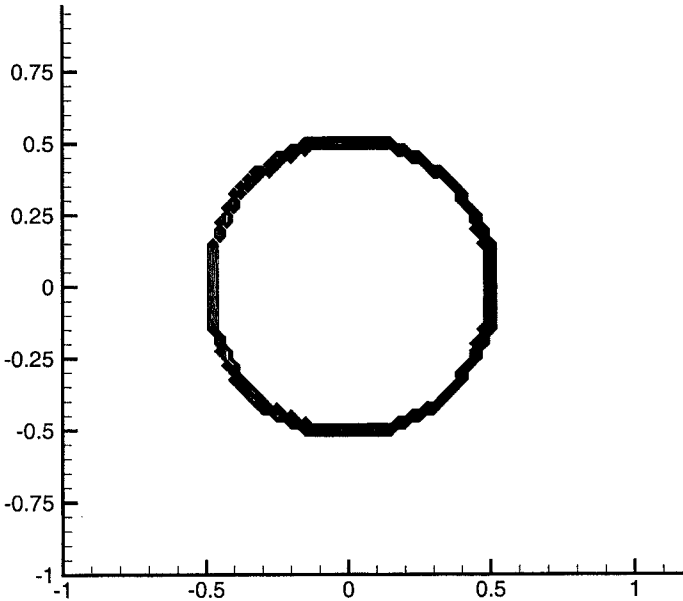


Fig. 2.6. Application of the enhanced edge detection method (2.10) and (2.11) for Example 2.2 using  $N = 80$  collocated Fourier coefficients in each fixed direction.

yielding

$$\begin{aligned}
 T_N(S_N^\sigma[f])(x(\bar{y})) &= \begin{cases} S_N^\sigma[f](x(\bar{y})), & \text{if } |T_x| > J_{\text{crit}} \\ 0, & \text{if } |T_x| < J_{\text{crit}} \end{cases} \\
 T_N(S_N^\sigma[f])(y(\bar{x})) &= \begin{cases} S_N^\sigma[f](y(\bar{x})), & \text{if } |T_y| > J_{\text{crit}} \\ 0, & \text{if } |T_y| < J_{\text{crit}} \end{cases}
 \end{aligned} \tag{2.11}$$

which pinpoints the jump locations for fixed values of  $\bar{x}$  and  $\bar{y}$ . The results are displayed in Fig. 2.6.

The limitations of the ‘‘Cartesian’’ detection done dimension by dimension are clear. Resolution is lost when the edges are not orthogonal to the Cartesian grid. This will have minor implications on high resolution reconstruction methods, as seen in Figs. 3.5 and 4.4, since the edges are determined only within a grid cell of the fixed variables.

### 3. RECONSTRUCTION OF PIECEWISE SMOOTH FUNCTIONS FROM SPECTRAL DATA

Various types of reconstruction methods for piecewise smooth functions from spectral data have been developed (consult, for example, [4, 6, 13, 16,

and 22]) with varying degrees of success. Higher resolution methods, critical for many scientific applications, can be used only when the jump locations of the function are pre-determined. Once the locations of the jump discontinuities are secured, computational costs, simplicity of algorithms, and robustness are the remaining critical components in choosing the optimal high resolution reconstruction method. In this section a procedure is developed that combines the simplicity of exponential filtering in smooth regions away from discontinuities and the highly resolved Gegenbauer reconstruction method in regions close to the discontinuities. This hybrid approach is less computationally intensive and costly, but still provides exponential accuracy in the maximum norm. We begin by reviewing the features of exponential filtering and the Gegenbauer reconstruction method for piecewise smooth functions.

### 3.1. Exponential Filtering

One might view the Gibbs phenomenon as a result of the slow decay rate of the expansion coefficients. Exponential filtering is a way to increase the decay rate by attenuating the high order coefficients. The filtered Fourier partial sum is computed as

$$f_N^\sigma(x) = \sum_{k=-N}^N \sigma_k \hat{f}_k e^{ik\pi x} \quad (3.1)$$

The filter  $\sigma(\eta) = \sigma(k/N)$  is defined as

$$\sigma(\eta) = e^{-\alpha |\eta|^p} \quad (3.2)$$

where  $p$  represents the order of the filter and  $\alpha$  measures the strength of the filter, generally chosen so that  $\sigma(1) \approx 0$  with machine accuracy. In all of the following examples,  $\alpha = 32$  was chosen. Exponential filtering is a popular tool in many scientific problems because of its robustness and simplicity. Other spectral expansions have similarly designed filters.

While filtering greatly improves the accuracy away from the discontinuities, the loss of information from the high order coefficients causes smearing over the discontinuities and resolution is severely compromised. On the other hand, high order filtering will retain the critical high resolution near the jump discontinuities but does not satisfactorily remove the Gibbs oscillations. These behaviors are demonstrated in Fig. 3.1. Figure 3.2 shows the convergence rate for increased number of coefficients and the errors of exponential filters of different orders. Clearly filtering is not suitable for applications requiring high resolution solutions that are free from Gibbs oscillations.

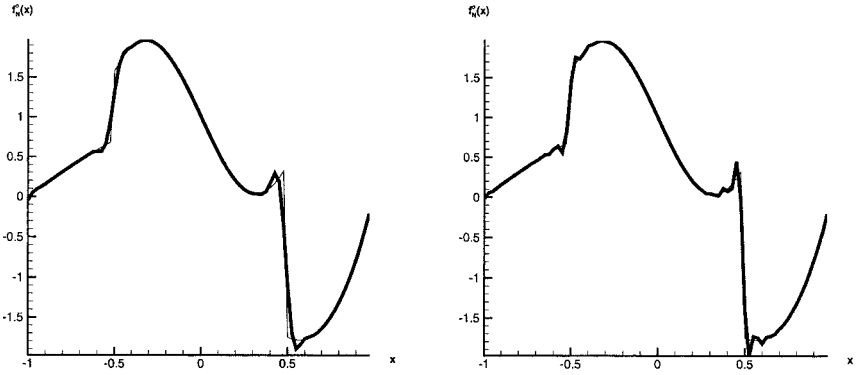


Fig. 3.1. The filtered Fourier partial sum with (a)  $p = 4$  and (b)  $p = 10$  applied to Example 2.1 using 80 Fourier collocated coefficients.

### 3.2. The Gegenbauer Reconstruction Method

The Gegenbauer reconstruction method was developed in [15] and extended in a litany of articles (consult [13] for references). It is a powerful tool that recovers spectral accuracy *up to* the discontinuity points in each smooth sub-interval of a piecewise analytic function by first converting the given spectral coefficients to Gegenbauer coefficients and then computing the Gegenbauer spectral projections in each smooth subinterval. The approximations in each sub-interval are subsequently “glued” together to form a spectrally accurate representation over the entire domain of the

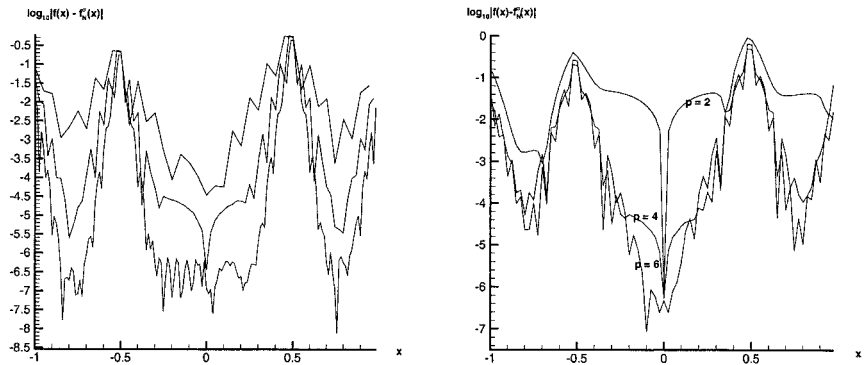


Fig. 3.2. Logarithmic pointwise errors for the filtered Fourier partial sum applied to Example 2.1 for (a) a fourth order filter using 40, 80, and 160 collocation points and (b) filters of orders  $p = 2, 4, 8$  with 80 Fourier collocated coefficients.

original piecewise smooth function. A detailed analysis of the Gegenbauer reconstruction method summarized below can be found in [13].

We begin by recalling the Gegenbauer partial sum expansion which converges exponentially for a smooth function  $f(x)$ , defined in  $[-1, 1]$ ,

$$f_m(x) = \sum_{l=0}^m \hat{f}_l^\lambda C_l^\lambda(x) \quad (3.3)$$

where  $\hat{f}_l^\lambda$  are the Gegenbauer coefficients defined by

$$\hat{f}_l^\lambda = \frac{1}{h_l^\lambda} \int_{-1}^1 (1-x^2)^{\lambda-1/2} C_l^\lambda(x) f(x) dx \quad (3.4)$$

The Gegenbauer polynomials,  $C_l^\lambda(x)$ , are orthogonal under the weight function  $(1-x^2)^{\lambda-1/2}$  with

$$\int_{-1}^1 (1-x^2)^{\lambda-1/2} C_k^\lambda(x) C_n^\lambda(x) dx = \delta_{k,n} h_n^\lambda, \quad h_n^\lambda = \pi^{1/2} C_n^\lambda(1) \frac{\Gamma(\lambda+1/2)}{\Gamma(\lambda)(n+\lambda)}$$

Now let  $f(x)$  be a piecewise smooth  $L_1$  function defined in  $[-1, 1]$  that is analytic in the sub-interval  $[a, b]$ . The interval of smoothness can be effectively determined by the edge detection and enhancement procedures described in Section 2. By defining a local variable  $\xi$  such that  $x(\xi) = \varepsilon\xi + \delta$ , where  $\varepsilon = (b-a)/2$  and  $\delta = (b+a)/2$ , the Gegenbauer partial sum expansion of  $f(x)$  in  $[a, b]$  can be written as

$$f_m(x(\xi)) = \sum_{l=0}^m \hat{f}_{l,\varepsilon}^\lambda C_l^\lambda(\xi), \quad -1 \leq \xi \leq 1 \quad (3.5)$$

where the Gegenbauer coefficients  $\hat{f}_{l,\varepsilon}^\lambda$  are defined by

$$\hat{f}_{l,\varepsilon}^\lambda = \frac{1}{h_l^\lambda} \int_{-1}^1 (1-\xi^2)^{\lambda-1/2} C_l^\lambda(\xi) f(\varepsilon\xi + \delta) d\xi \quad (3.6)$$

As shown in [13], an exponentially accurate approximation to  $\hat{f}_{l,\varepsilon}^\lambda$  can be constructed as

$$\hat{g}_{l,\varepsilon}^\lambda = \frac{1}{h_l^\lambda} \int_{-1}^1 (1-\xi^2)^{\lambda-1/2} C_l^\lambda(\xi) f_N(\varepsilon\xi + \delta) d\xi \quad (3.7)$$

based on the spectral partial sum expansion,  $f_N(\varepsilon\xi + \delta)$ . This approximation can then be used to replace  $\hat{f}_{l,\varepsilon}^\lambda$  in the computation of the Gegenbauer partial sum. Specifically,

$$g_m^\lambda(x(\xi)) = \sum_{l=0}^m \hat{g}_{l,\varepsilon}^\lambda C_l^\lambda(\xi) \tag{3.8}$$

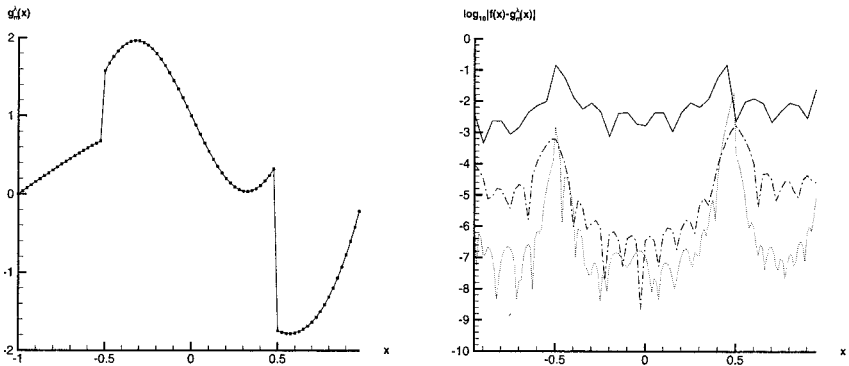
forms an exponentially convergent approximation to  $f(x)$  in  $[a, b]$  in the maximum norm provided that the Gegenbauer parameters are suitably chosen with  $m, \lambda \sim \varepsilon N$ .

Figure 3.3 demonstrates the effectiveness of the Gegenbauer reconstruction method using the pseudospectral Fourier partial sum approximation

$$f_N(\varepsilon\xi + \delta) = \sum_{k=-N}^N \tilde{f}_k e^{ik\pi(\varepsilon\xi + \delta)}, \quad \tilde{f}_k = \frac{1}{2N} \sum_{j=0}^{2N-1} f(z_j) e^{-ik\pi z_j} \tag{3.9}$$

where  $z_j = -1 + (j/N), j = 0, \dots, 2N - 1$ . Use of other (pseudo-)spectral partial sum expansions also yield the exponentially convergent approximations (3.7) and (3.8). For example, one may use the Legendre partial sum approximation

$$f_N(\varepsilon\xi + \delta) = \sum_{k=0}^N \tilde{f}_k P_k(\varepsilon\xi + \delta) \tag{3.10}$$



**Fig. 3.3.** Gegenbauer reconstruction method applied to Example 2.1, with  $m = \lambda = 0.4\varepsilon N$  using (a)  $2N = 80$  Fourier collocated coefficients. (b) Logarithmic pointwise errors for 40, 80, and 160 collocation points.

where the pseudo-spectral coefficients are computed as

$$\tilde{f}_k = \frac{1}{\gamma_k} \sum_{j=0}^N f(z_j) P_k(z_j) w_j \quad (3.11)$$

based on the Gauss quadrature nodes  $z_j$ ,  $j=0, \dots, N$ , the appropriate normalization factor  $\gamma_k$ , and weight function  $w_j$ .

The two dimensional Gegenbauer approximation is a direct extension of the one dimensional case and is written as

$$g_{m_1, m_2}^{\lambda_1, \lambda_2}(x(\xi_x), y(\xi_y)) = \sum_{l_1=0}^{m_1} \sum_{l_2=0}^{m_2} \hat{g}_{l_1, l_2}^{\lambda_1, \lambda_2} C_{l_1}^{\lambda_1}(\xi_x) C_{l_2}^{\lambda_2}(\xi_y) \quad (3.12)$$

with

$$\begin{aligned} \hat{g}_{l_1, l_2}^{\lambda_1, \lambda_2} = & \frac{1}{h_{l_1}^{\lambda_1}} \frac{1}{h_{l_2}^{\lambda_2}} \int_{-1}^1 \int_{-1}^1 (1 - \xi_x^2)^{\lambda_1 - 1/2} (1 - \xi_y^2)^{\lambda_2 - 1/2} C_{l_1}^{\lambda_1}(\xi_x) \\ & \times C_{l_2}^{\lambda_2}(\xi_y) f_N(\varepsilon_x \xi_x + \delta_x, \varepsilon_y \xi_y + \delta_y) d\xi_x d\xi_y \end{aligned}$$

Figure 3.4 shows the two dimensional Gegenbauer approximation of Example 2.2 using the pseudo-spectral Fourier coefficients. Figure 3.5 shows the one dimensional cross sections of the two dimensional Gegenbauer reconstruction. In this example, the edge detection (2.8) and enhancement (2.11) techniques were used to obtain the regions of smoothness before utilizing the Gegenbauer reconstruction method. The effects of the ‘‘Cartesian’’ edge detection procedure are evident in Fig. 3.5 where the reconstruction is exponentially accurate up to the grid cell of the jump discontinuity.

### 3.3. Computational Considerations for the Gegenbauer Reconstruction Method

It is clear that the Gegenbauer reconstruction method yields remarkably highly resolved approximations without the negative effects of the Gibbs phenomenon. Still, computational costs and robustness must be considered carefully if the method is to have broad scientific impact. We first consider the issue of cost.

In the case where the Fourier (pseudo-)spectral approximation (3.9) is utilized in the construction of the Gegenbauer coefficients,

$$\hat{g}_{l, \varepsilon}^{\lambda} = \frac{1}{h_l^{\lambda}} \int_{-1}^1 (1 - \xi^2)^{\lambda - 1/2} C_l^{\lambda}(\xi) \sum_{k=-N}^N \tilde{f}_k e^{ik\pi(\varepsilon\xi + \delta)} d\xi$$

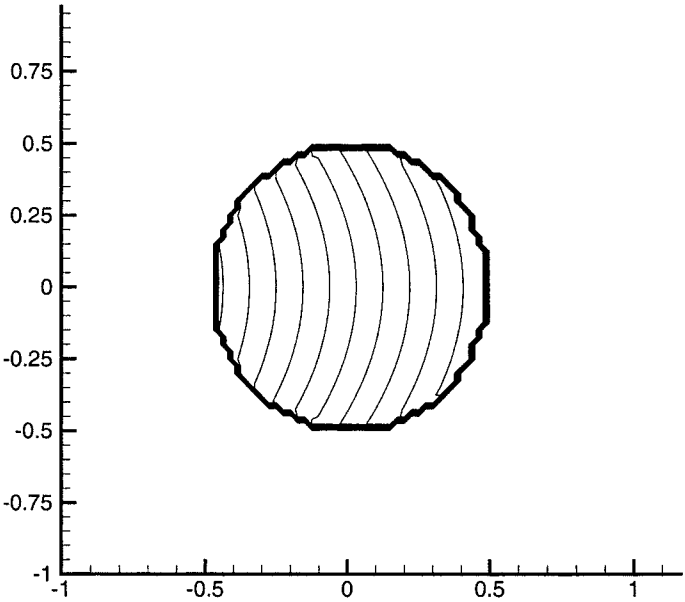


**Fig. 3.4.** Contour plot of Example 2.2 using the two dimensional Gegenbauer reconstruction method (3.12) based on  $2N = 80$  pseudo-spectral Fourier coefficients in each direction. Here  $m_1 = m_2 = 6$ , and  $\lambda_1 = \lambda_2 = 8$ .

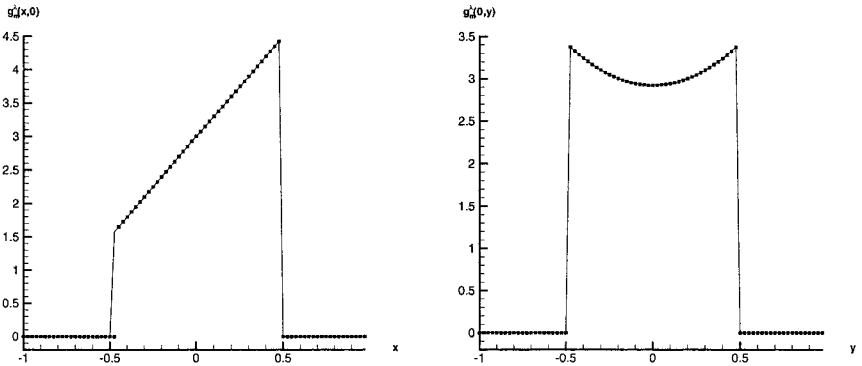


**Fig. 3.5.** Cross sections of the two dimensional Gegenbauer approximation (dots) in the (a)  $x$  and (b)  $y$  directions.

the explicit expression [2]

$$\frac{1}{h_l^\lambda} \int_{-1}^1 (1 - \xi^2)^{\lambda-1/2} C_l^\lambda(\xi) e^{ik\pi(\varepsilon\xi + \delta)} d\xi = \Gamma(\lambda) \left(\frac{2}{\pi k}\right)^\lambda i^l (l + \lambda) J_{l+\lambda}(\pi k)$$

is exploited to obtain

$$\hat{g}_{l,\varepsilon}^\lambda = \delta_{0,l} \tilde{f}_0 + \Gamma(\lambda) i^l (l + \lambda) \sum_{0 < |k| \leq N} J_{l+\lambda}(\pi k \varepsilon) \left(\frac{2}{\pi k \varepsilon}\right)^\lambda \tilde{f}_k e^{ik\pi\delta} \quad (3.13)$$

This allows use of the efficient FFT algorithm and avoids the more expensive quadrature formulation. Some additional cost is incurred in the two dimensional case.

Unfortunately other spectral expansions, e.g., the Legendre expansion, do not lend themselves to such clean formulations as in (3.13), and we are forced to address the computational costs of integrating  $\hat{g}_{l,\varepsilon}^\lambda$ . Consider, as an example, the application of the Chebyshev Gauss–Lobatto quadrature formula for (3.7), which yields the approximation

$$\hat{g}_{l,\varepsilon}^\lambda = \frac{1}{h_l^\lambda} \frac{\pi}{\bar{N}} \sum_{j=0}^{\bar{N}} \frac{1}{c_j} f_N(\varepsilon \xi_j + \delta) (1 - \xi_j^2)^\lambda C_l^\lambda(\xi_j)$$

$$c_j = \begin{cases} 1, & \text{if } j = 1, \dots, \bar{N} - 1 \\ 2, & \text{if } j = 0 \text{ or } j = \bar{N} \end{cases}$$

where  $f_N(\varepsilon \xi_j + \delta)$  is computed by (3.10) on the points  $\xi_j = \cos(j\pi/N)$ ,  $j = 0, \dots, \bar{N}$ , and  $\bar{N} \geq N + 2\lambda + m$ . This leads to the Gegenbauer approximation

$$g_m(x(\xi)) = \sum_{l=0}^m \frac{1}{h_l^\lambda} \frac{\pi}{\bar{N}} \sum_{j=0}^{\bar{N}} \frac{1}{c_j} f_N(\varepsilon \xi_j + \delta) (1 - \xi_j^2)^\lambda C_l^\lambda(\xi_j) C_l^\lambda(\xi)$$

Our goal is to reduce the computational effort in computing the Gegenbauer approximation. We start by reformulating the Gegenbauer approximation as

$$g_m(x(\xi)) = \frac{\pi}{\bar{N}} \sum_{j=0}^{\bar{N}} \frac{1}{c_j} f_N(\varepsilon \xi_j + \delta) (1 - \xi_j^2)^\lambda \sum_{l=0}^m \frac{C_l^\lambda(\xi_j) C_l^\lambda(\xi)}{h_l^\lambda}$$

Recall the Christoffel–Darboux formula for Gegenbauer polynomials,

$$\sum_{l=0}^m \frac{C_l^\lambda(\xi_j) C_l^\lambda(\xi)}{h_l^\lambda} = \frac{k_m}{k_{m+1} h_m^\lambda} \frac{C_{m+1}^\lambda(\xi_j) C_m^\lambda(\xi) - C_m^\lambda(\xi_j) C_{m+1}^\lambda(\xi)}{\xi_j - \xi}$$

where

$$k_m = \frac{2^m \Gamma(\lambda + m)}{m! \Gamma(\lambda)}$$

The Christoffel–Darboux formula allows the elimination of one sum from the computation to obtain

$$g_m(x(\xi)) = \frac{\pi}{\bar{N}} \frac{k_m}{k_{m+1} h_m^\lambda} \sum_{j=0}^{\bar{N}} \frac{1}{c_j} f_N(\varepsilon \xi_j + \delta) (1 - \xi_j^2)^\lambda \times \frac{C_{m+1}^\lambda(\xi_j) C_m^\lambda(\xi) - C_m^\lambda(\xi_j) C_{m+1}^\lambda(\xi)}{\xi_j - \xi} \tag{3.14}$$

If  $\xi = \xi_j$ , then applying the equality  $2\lambda C_{m-1}^{\lambda+1}(\xi) = dC_m^\lambda(\xi)/d\xi$  gives

$$g_m(x(\xi_j)) = \frac{\pi}{\bar{N}} \frac{k_m}{k_{m+1} h_m^\lambda} \sum_{j=0}^{\bar{N}} \frac{1}{c_j} f_N(\varepsilon \xi_j + \delta) (1 - \xi_j^2)^\lambda \times 2\lambda (C_{m+1}^{\lambda+1}(\xi_j) C_m^\lambda(\xi_j) - C_{m+1}^\lambda(\xi_j) C_{m-1}^{\lambda+1}(\xi_j))$$

While manipulating the Christoffel–Darboux formula reduces the computational expense, there is still the issue of the Gegenbauer reconstruction method’s susceptibility to round-off error. The Gegenbauer polynomials grow very rapidly, for instance  $C_m^\lambda(1) = \Gamma(m + 2\lambda)/m! \Gamma(2\lambda)$ . Hence not only is the theoretical exponential convergence obtained for  $m, \lambda \sim \varepsilon N$  unrealizable, but the round-off error may completely ruin the approximation. Additionally, improving the computational cost (3.14) further exacerbates the situation since the Gegenbauer polynomials are multiplied together in the Christoffel–Darboux formula.

To temper this effect we introduce two modifications of the Gegenbauer polynomials:

$$\begin{aligned} C_{S,m}^\lambda(\xi) &= S C_m^\lambda(\xi) \\ C_{\bar{N},m}^\lambda(\xi) &= \frac{1}{\bar{N}} C_m^\lambda(\xi_j) \end{aligned} \tag{3.15}$$

where we have defined

$$S := S(m, \lambda) = \frac{\pi k_m}{k_{m+1} h_m^\lambda} = \frac{\Gamma(m)}{\Gamma(m + 2\lambda - 1)} 4^{\lambda-1} (\Gamma(\lambda))^2 \tag{3.16}$$

Note that  $S$  and  $\bar{N}$  are fixed once the parameters  $m$  and  $\lambda$  have been chosen and do not change in the computation of (3.15). Clearly  $S$  and  $1/\bar{N}$  are small and decreasing values with respect to  $m$ ,  $\lambda$ , and  $N$ . This is extremely helpful in preventing numerical round-off error when computing the Gegenbauer polynomials. The approximation (3.14) now reads

$$g_m(x(\zeta)) = \sum_{j=0}^{\bar{N}} \frac{f_N(\varepsilon \zeta_j + \delta)(1 - \zeta_j^2)^\lambda}{c_j} \times \left[ \frac{C_{\bar{N}, m+1}^\lambda(\zeta_j) C_{S, m}^\lambda(\zeta) - C_{\bar{N}, m}^\lambda(\zeta_j) C_{S, m+1}^\lambda(\zeta)}{\zeta_j - \zeta} \right] \quad (3.17)$$

Figure 3.6 demonstrates the effectiveness of the modified Gegenbauer approximation (3.17) using the Legendre pseudo-spectral partial sum approximation. The Gegenbauer reconstruction method is now much more robust and cost effective, making it more applicable to problems of greater variation.

### 3.4. The Hybrid Approach

As indicated in Figs. 3.3 and 3.6, both formulations (3.13) and (3.17) provide robust computational reconstruction procedures for piecewise analytic functions. Although the cost is significantly diminished, the reconstruction is still considerably expensive for problems in higher dimensions. To treat this issue, we introduce a new hybrid approach that combines the simplicity of exponential filtering in smooth regions away from discontinuities and the highly resolved Gegenbauer reconstruction method in

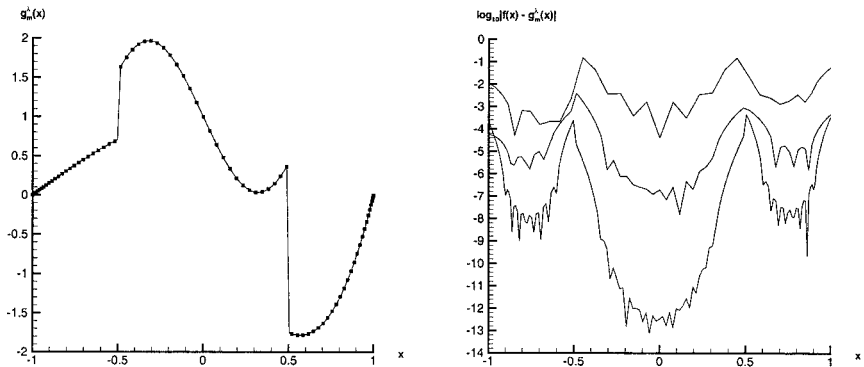


**Fig. 3.6.** Gegenbauer reconstruction method applied to Example 2.1, with  $m = 0.2\varepsilon N$ ,  $\lambda = 0.4\varepsilon N$ . (a) Approximation using  $N = 80$  Legendre Gauss quadrature points. (b) Logarithmic pointwise errors for 40, 80, and 160 collocation points.

regions close to the discontinuities. Specifically, if  $f(x)$  is smooth inside the interval  $[a, b]$  then

$$g_m^{\sigma, \lambda}(x) = \begin{cases} g_m^\lambda(x), & \text{if } a \leq x \leq a + \rho \text{ or } b - \rho \leq x \leq b \\ f_N^\sigma(x), & \text{if } a + \rho < x < b - \rho \end{cases} \quad (3.18)$$

where  $0 \leq \rho \leq (b - a)/2$  is a neighborhood parameter determined for each particular application. Clearly, higher accuracy is obtained for larger values of  $\rho$  since the Gegenbauer reconstruction method would be used in a larger part of the sub-interval. In this case, a higher order filter for reconstruction in the region  $a + \rho < x < b - \rho$  should be chosen since the Gibbs oscillations seen in Fig. 3.1 will be removed by the application of the Gegenbauer reconstruction method in the regions close to the jump discontinuities. On the other hand, choosing smaller  $\rho$  would significantly lessen the computational expense. For the many computational problems having very refined grids, one is forced to use small  $\rho$  because of the high cost of the Gegenbauer reconstruction method. It is also reasonable to choose  $\rho = \rho(x)$ , since it is likely that some sub-interval reconstructions demand higher resolution reconstruction than others. For instance, in MRI images, it is sometimes desirable to resolve the image near the skull bone, but some of the finer features on the interior can be smoothed over. This particular example will be discussed in Section 4.

#### 4. NUMERICAL APPLICATIONS

To demonstrate the efficacy of the hybrid Gegenbauer reconstruction method, we return to Example 2.1. It is clear from Figs. 4.1 and 4.2 that the

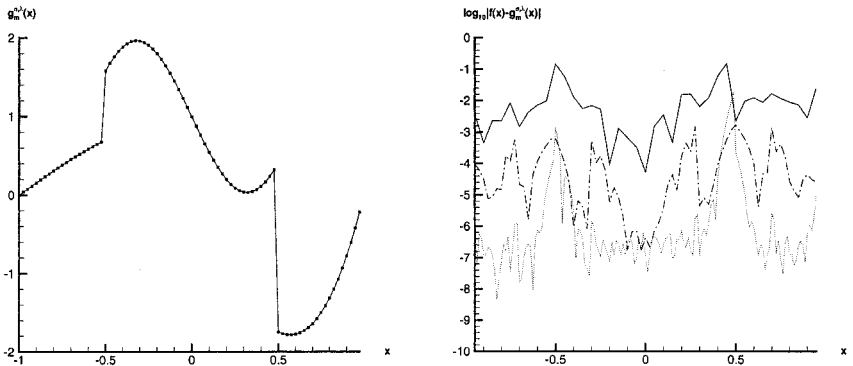


**Fig. 4.1.** The hybrid Gegenbauer reconstruction method applied to Example 2.1, with  $\rho = 0.2$  and  $m = \lambda = 0.4\epsilon N$  using (a) the Fourier partial sum expansion with 80 collocation points. (b) Logarithmic pointwise errors for 40, 80, and 160 collocation points.

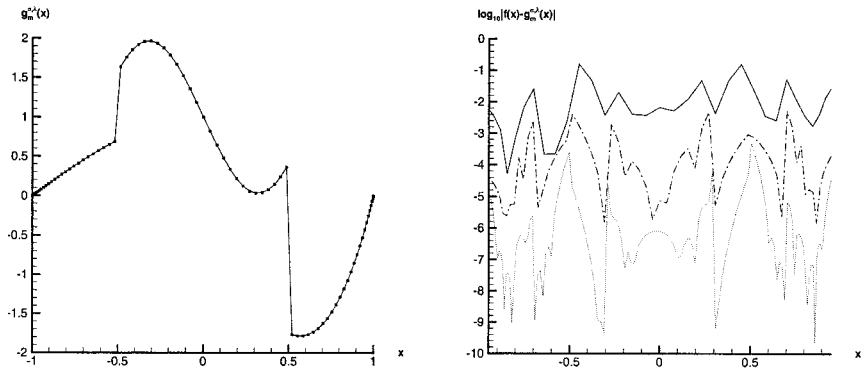


**Fig. 4.2.** Hybrid Gegenbauer reconstruction method applied to Example 2.1, with  $m = 0.2\epsilon N$  and  $\lambda = 0.4\epsilon N$  using (a) the Legendre partial sum expansion with  $N = 80$  points (b) logarithmic pointwise errors for 40, 80, and 160 points.

hybrid method recovers piecewise smooth functions with high accuracy up to the points of discontinuity. In both cases, the hybrid neighborhood parameter  $\rho = 0.2$  and filter parameters  $p = 6$  and  $\alpha = 32$  were used. Although some loss of accuracy is seen away from the discontinuities, the overall convergence rate is still very high.

The hybrid Gegenbauer reconstruction method is well suited for the two dimensional case. The procedure can be applied with the Fourier or Legendre partial sum expansion in either or both directions. Figures 4.3 and 4.4 compare the hybrid method applied to Example 2.2 using the

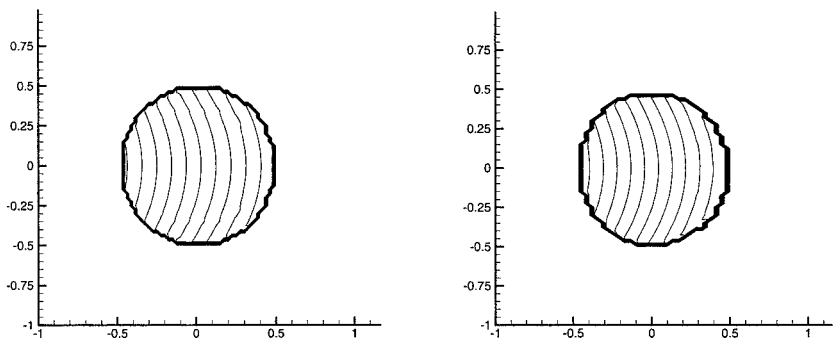


**Fig. 4.3.** Contour plot of Example 2.2 approximated by the two dimensional hybrid Gegenbauer reconstruction method using (a) the Fourier partial sum expansion in both directions and (b) the Legendre partial sum expansion in the  $x$  direction and the Fourier partial sum expansion in the  $y$  direction with 80 collocation points in each direction and parameters  $m_1 = m_2 = 6$ , and  $\lambda_1 = \lambda_2 = 8$ .

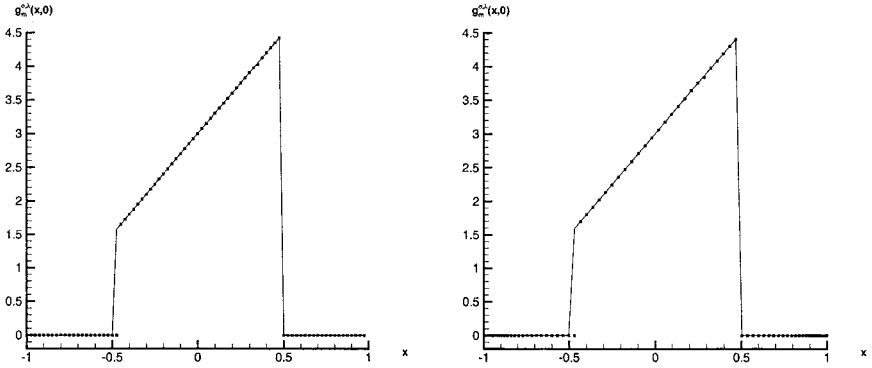


**Fig. 4.4.** Cross section of the hybrid Gegenbauer approximation of Example 2.2 in the  $x$  direction using (a) the Fourier partial sum expansion in both directions and (b) the Legendre partial sum expansion in the  $x$  direction and the Fourier partial sum expansion in the  $y$  direction with 80 collocation points in each direction and parameters  $m_1 = m_2 = 6$ , and  $\lambda_1 = \lambda_2 = 8$ .

Fourier partial sum expansion in both directions with the hybrid method using the Legendre partial sum in the  $x$  direction and the Fourier partial sum in the  $y$  direction. In both cases the hybrid neighborhood parameter  $\rho = 0.2$  and filter parameters  $p = 6$  and  $\alpha = 32$  were used.

One important application of reconstruction methods is in post-processing numerical solutions of partial differential equations. For example, in the case of hyperbolic conservation laws, the solution develops shock discontinuities which lead to the undesirable Gibbs phenomenon. Much research has been devoted to creating numerical spectral methods that reduce the effects of the Gibbs phenomenon. For example, the spectral viscosity (SV) method, which originated in [21] and developed further to include non-periodic problems in [18], recovers spectrally accurate approximations to the projections of the entropy solutions. However, due to the shocks in the solution, even the exact projection of the entropy solution would suffer from the Gibbs phenomenon, and hence a post-processing reconstruction procedure is required.

The Gegenbauer reconstruction method has been shown to effectively post-process the SV solution [10], [20]. To demonstrate the efficacy of the hybrid Gegenbauer reconstruction method as a post-processor for piecewise smooth solutions, we consider the dam break problem.

**Example 4.1 (One-dimensional dam break problem).** Consider the hyperbolic conservation law,

$$\frac{\partial}{\partial t} \mathbf{q} + \frac{\partial}{\partial x} \mathbf{f}(\mathbf{q}) = 0 \tag{4.1}$$

with vector of variables and the flux vector given by

$$\mathbf{q} = \begin{pmatrix} uh \\ h \end{pmatrix}, \quad \mathbf{f} = \begin{pmatrix} u^2h + 1/2gh^2 \\ uh \end{pmatrix}$$

Here  $h = h(x, t)$  is the height of the free upper surface,  $u = u(x, t)$  is the (depth-averaged) fluid velocity and  $g$  is the acceleration due to gravity. The fluid is initially at rest both sides of a dam located at  $x = 0$ . At time  $t = 0$  a dam break is simulated by suddenly removing the dam wall. Initial conditions are given as

$$h(x, 0) = \begin{cases} h_0, & x < 0 \\ h_1, & x > 0 \end{cases}$$

$$u(x, 0) = 0$$

for specified  $h_0$  and  $h_1$ .

The analytical solution consists of a shock front (or “bore”) propagating to the right and a rarefaction wave propagating to the left. One particular solution is shown in Fig. 4.5.

Since the solution also contains discontinuities in the derivative, high resolution post-processing reconstruction requires the locations of the discontinuities in the derivatives as well (consult [10]). Results from employing the hybrid Gegenbauer reconstruction method directly to the exact solution are shown in Fig. 4.6, where the Legendre partial sum expansion was used to build the Gegenbauer coefficients.

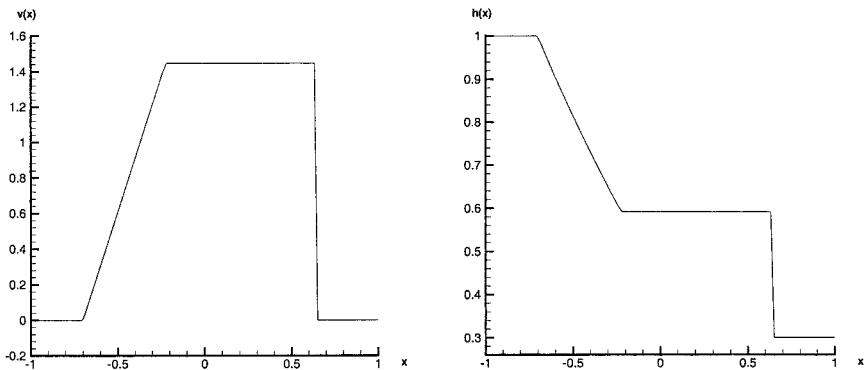


**Fig. 4.5.** The exact (a) velocity and (b) height solutions for the dam break problem with initial conditions  $h_0 = 1$  and  $h_1 = 0.8$  at time  $T = 0.15$ .

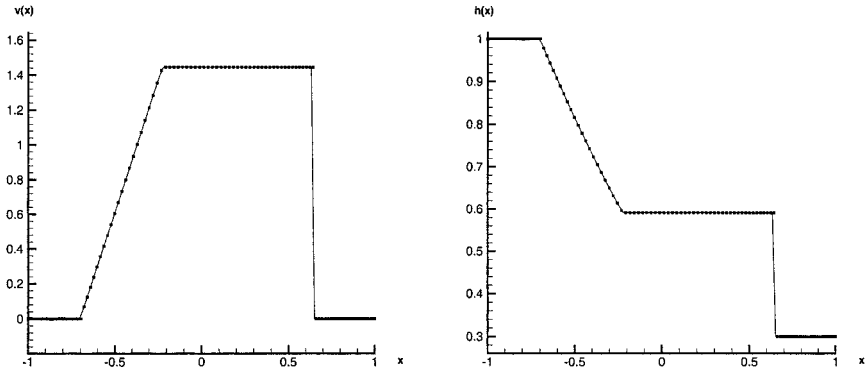


**Fig. 4.6.** The hybrid Gegenbauer reconstruction method applied to the exact solution of the dam break problem with  $N=128$  Gauss quadrature points and  $m=\lambda=0.2\varepsilon N$ . the hybrid neighborhood parameter  $\rho=0.2$  and filter parameters  $p=6$  and  $\alpha=32$  were used. Shown is (a) the velocity profile and (b) the height profile.

As evident in Fig. 4.7, the SV solution of a hyperbolic conservation law is riddled with noisy oscillations due to the Gibbs phenomenon. Nevertheless, the hybrid Gegenbauer reconstruction method recovers a highly accurate approximation from the SV solution without oscillations or the undesirable smearing seen in other post-processing reconstruction methods. The results are shown in Fig. 4.8.

Computer tomography serves as an excellent example for the application of the hybrid Gegenbauer method. A tomography image is reconstructed from its X-ray projections, which are constructed by the Radon transform of the image function. The close relationship between the Radon and

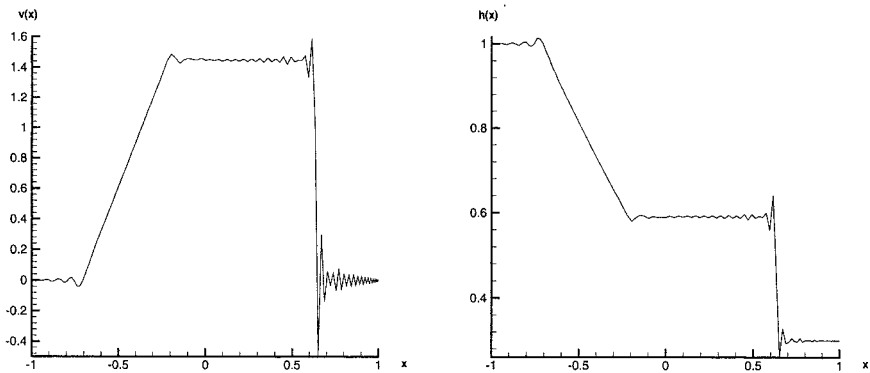


**Fig. 4.7.** The SV solution of the dam break problem with  $N=128$  Gauss quadrature points. Shown is (a) the velocity profile and (b) the height profile.

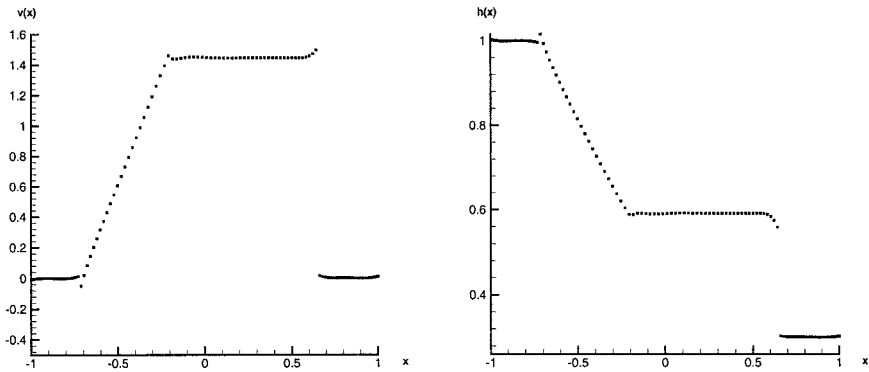
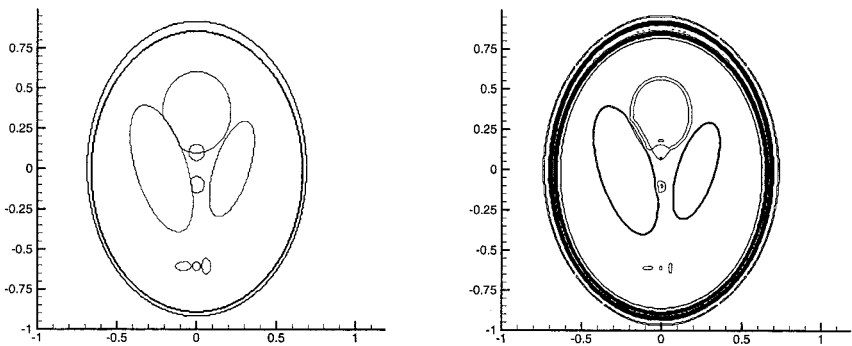


**Fig. 4.8.** The hybrid Gegenbauer reconstruction method applied to the SV solution of the dam break problem with  $N = 128$  Gauss quadrature points and  $\rho = 0.2$  and  $m = \lambda = 0.2\varepsilon N$ . the hybrid neighborhood parameter  $\rho = 0.2$  and filter parameters  $p = 6$  and  $\alpha = 32$  were used. Shown is (a) the velocity profile and (b) the height profile.

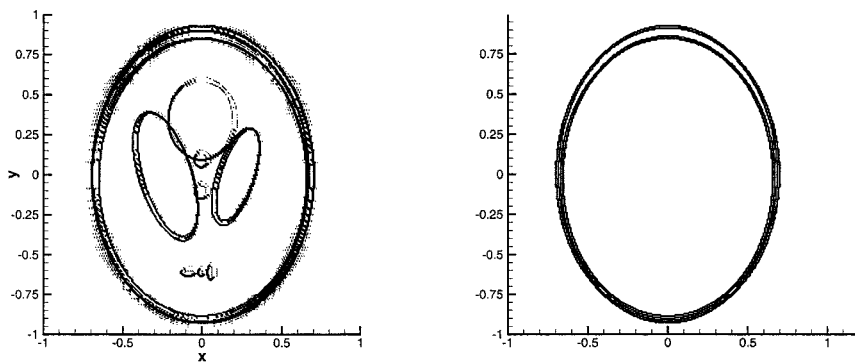
Fourier transform dictates the suitability of Fourier spectral methods to computer tomography problems.

Figure 4.9 shows the image of the piecewise constant Shepp–Logan phantom brain on a  $[256 \times 256]$  grid domain and its corresponding filtered Fourier spectral representation. Here the Fourier coefficients are computed directly from the phantom image. Numerical algorithms for the conversion of the Radon to Fourier coefficients can be found in [11].

A high resolution reconstruction method is ideal for the Shepp–Logan phantom image since the filtered Fourier approximation, shown in Fig. 4.9, neither satisfactorily removes the Gibbs phenomenon nor resolves the region near the skull bone. As previously discussed, the edges of the image



**Fig. 4.9.** (a) The phantom image using a  $256 \times 256$  size mesh. (b) The pseudo-spectral filtered approximation of the phantom image.



**Fig. 4.10.** (a) The concentration method (2.8) and (b) the enhanced edge detection procedure (2.11) applied to the Shepp-Logan phantom image.

must be determined before applying a high resolution reconstruction method. Figure 4.10 demonstrates the use of the concentration method (2.8) and enhancement technique (2.11) to determine the edges of the Shepp-Logan phantom brain. In this case, one can choose the critical threshold in (2.11) to either include the edges of the interior structures or to dismiss them, depending on desired resolution. For simplicity we choose to ignore the edges of the interior structures.

The fine grid resolution makes the Gegenbauer reconstruction method unreasonably expensive to apply everywhere. Fortunately, the cost effective hybrid Gegenbauer reconstruction method can be applied to accurately recover the original Shepp-Logan phantom image. The results are displayed in Fig. 4.11. Since the interior of the phantom does not demand high resolution reconstruction, exponential filtering is used for the inside structures. The Gegenbauer method is applied to recover the phantom image near the skull bone, where high resolution is more critical. Note that for some additional cost, the procedure can be easily tuned to also obtain high resolution recovery on the interior structures.

## 5. CONCLUDING REMARKS

The hybrid Gegenbauer reconstruction method is an exceptionally accurate reconstruction procedure that combines the simplicity of exponential filtering away from the jump discontinuities with the highly resolved Gegenbauer reconstruction method in regions close to the discontinuities. The main reason for creating a hybrid method is to reduce the high cost incurred by the Gegenbauer reconstruction method.

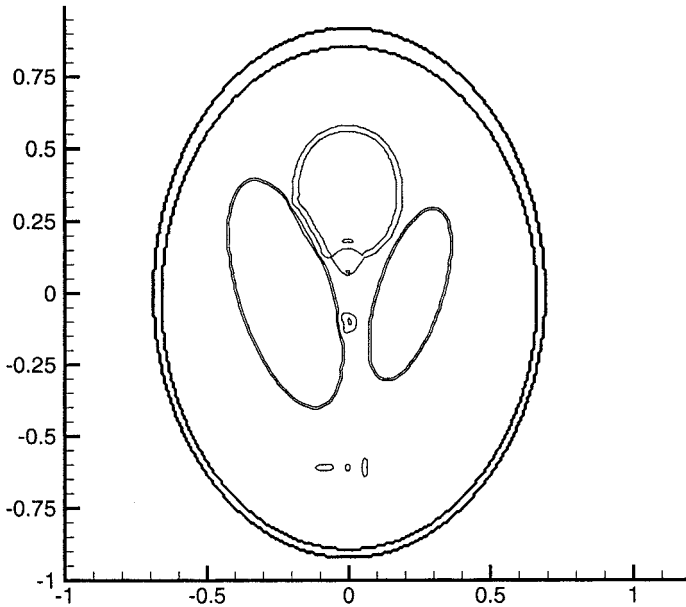


**Fig. 4.11.** The hybrid Gegenbauer reconstruction method applied to approximate the image of the Shepp–Logan phantom. Here  $\lambda_1 = \lambda_2 = 4$ ,  $m_1 = m_2 = 3$ , the hybrid neighborhood parameter  $\rho = 0.01$ , and the filter parameters  $p = 4$  and  $\alpha = 32$  were chosen.

By exploiting the relationship between the Gegenbauer coefficients computed from the Fourier partial sum expansion and the explicit formula involving the Bessel's function (3.13), the cost of the Gegenbauer reconstruction method is reduced for Fourier spectral methods. In this paper we introduced another way to decrease the cost of Gegenbauer reconstruction by taking advantage of the Christoffel–Darboux formula (3.14). This makes the Gegenbauer reconstruction method more feasible for other partial sum expansions (e.g., Legendre, Chebyshev) as well. A way to curtail round-off error was also addressed in (3.15).

The hybrid algorithm (3.18) is extremely useful for two dimensional problems with very refined grids where cost effectiveness becomes a critical issue. Numerical applications, such as the reconstruction of MRI images, serve as prime examples. Reconstructed images are highly resolved without using expensive and time consuming techniques. Future investigations include

- Optimization of parameters for the hybrid Gegenbauer reconstruction method. The regions of exponential filtering and Gegenbauer reconstruction are inherently problem dependent. However, the

order of the exponential filter is linked to the proximity of the jump discontinuity and could be determined independently. No optimization for the Gegenbauer parameters  $m$  and  $\lambda$  has yet been attempted.

- Round-off error. Some round-off error is still apparent as the grid becomes more refined. For instance, we used  $m = 0.4\epsilon N$  for examples with  $N < 80$  grid points, but accuracy is negatively impacted when  $N$  increases for corresponding values of  $m$ . Higher computer precision is the best course of action, but work can be done to improve the computational accuracy of the rapidly growing Gegenbauer polynomials.
- Edge detection in two dimensions. Current investigation is under way to develop a two-dimensional edge detection technique that is not subject to the limitations of “Cartesian” detection.
- Application of the hybrid Gegenbauer reconstruction method to real physical data. We are currently testing the hybrid Gegenbauer reconstruction method on real physical and simulated data, specifically on MRI and PET data which contain significant amounts of noise.

## ACKNOWLEDGMENT

This work was supported in part by the Sloan Foundation and the Arizona Alzheimer’s Research Collaborative funded by the Arizona department of health.

## REFERENCES

1. Banerjee, N. S., and Geer, J. (1995). Exponentially accurate approximations to piecewise smooth periodic functions, ICASE Report No. 95-17, NASA Langley Research Center.
2. Bateman, H. (1953). *Higher Transcendental Functions*, Vol. 2, McGraw-Hill.
3. Bauer, R. (1995). *Band Filters for Determining Shock Locations*, Ph.D. thesis, Applied Mathematics, Brown University.
4. Cai, W., Gottlieb, D., and Shu, C.-W. (1992). On one-sided filters for spectral Fourier approximations of discontinuous functions. *SIAM J. Numer. Anal.* **29**(4), 905–916.
5. Canuto, C., Hussaini, M. Y., Quarteroni, A., and Zang, T. A. (1987). *Spectral Methods in Fluid Dynamics*.
6. Eckhoff, K. S. (1995). Accurate reconstructions of functions of finite regularity from truncated series expansions. *Math. Comp.* **64**, 671–690.
7. Eckhoff, K. S. (1998). On a high order numerical method for functions with singularities. *Math. Comp.* **67**, 1063–1087.
8. Gelb, A., and Tadmor, E. (1999). Detection of edges in spectral data. *Appl. Comp. Harmonic Anal.* **7**, 101–135.
9. Gelb, A., and Tadmor, E. (2000). Detection of edges in spectral data II. Nonlinear enhancement. *SIAM J. Numer. Anal.* (in press).
10. Gelb, A., and Tadmor, E. (2000). Enhanced spectral viscosity approximations for conservation laws. *Appl. Numer. Math.* **33**, 3–21.

11. Gottlieb, D., Gustafsson, B., and Forssén, P. (2000). On the direct Fourier method for computer tomography. *IEEE Trans. Med. Imag.* **19**, 223–232.
12. Gottlieb, D., and Orszag, S. (1977). *Numerical Analysis of Spectral Methods: Theory and Applications*, SIAM-CBMS, Philadelphia.
13. Gottlieb, D., and Shu, C.-W. (1997). On the Gibbs phenomenon and its resolution. *SIAM Rev.* **39**, 644–668.
14. Gottlieb, D., and Shu, C.-W. (1995). On the Gibbs phenomenon IV. Recovering exponential accuracy in a subinterval from a Gegenbauer partial sum of a piecewise analytic function. *Math. Comp.* **64**, 1081–1095.
15. Gottlieb, D., Shu, C.-W., Solomonoff, A., and Vandeven, H. (1992). On The Gibbs phenomenon I. Recovering exponential accuracy from the Fourier partial sum of a non-periodic analytic function. *J. Comput. Appl. Math.* **43**, 81–92.
16. Gottlieb, D., and Tadmor, E. (1985). Recovering pointwise values of discontinuous data within spectral accuracy. In Murman, E. M., and Abarbanel, S. S. (eds.), *Progress and Supercomputing in Computational Fluid Dynamics*, Proceedings of a 1984 U.S.-Israel Workshop, Progress in Scientific Computing, Vol. 6, Birkhauser, Boston, pp. 357–375.
17. Kvernadze, G. (1998). Determination of the jump of a bounded function by its Fourier series. *J. Approx. Theory* **92**, 167–190.
18. Maday, Y., Ould Kaber S. M., and Tadmor, E. (1993). Legendre pseudospectral viscosity method for nonlinear conservation laws. *SIAM J. Numer. Anal.* **30**, 321–342.
19. Mhaskar, H. N., and Prestin, J. (2000). On the detection of singularities of a periodic function, preprint.
20. Shu, C.-W., and Wong, P. (1995). A note on the accuracy of spectral method applied to nonlinear conservation laws. *J. Sci. Comput.* **10**, 357–369.
21. Tadmor, E. (1989). Convergence of spectral methods for nonlinear conservation laws. *SIAM J. Numer. Anal.* **26**, 30–44.
22. Vandeven, H. (1991). Family of spectral filters for discontinuous problems. *SIAM J. Sci. Comput.* **48**, 159–192.